Filtering Integration Schemes Based on the Laplace and Z Transforms

PETER LYNCH

Irish Meteorological Service, Dublin, Ireland

(Manuscript received 29 May 1990, in final form 10 September 1990)

ABSTRACT

A filtering integration scheme based on a modification of the inversion integral for the Laplace transform (LT) is developed and implemented in a barotropic limited-area model. The LT scheme is compared to a conventional scheme and shown to simulate faithfully the low-frequency evolution of the atmosphere while eliminating high-frequency oscillations. The scheme is combined with a Lagrangian treatment of advection giving stable integrations for long time steps.

Simple perturbation experiments show that the LT model can absorb an imposed disturbance without data shock. It is superior in this respect to more conventional schemes and may prove useful for asynoptic data assimilation.

An alternative formulation of the filtering scheme using the Z transform is described. This technique is applied to a system of equations that have been discretized with respect to time. The Z-transform scheme is shown to behave in a manner similar to the Laplace-transform scheme.

1. Introduction

The primitive equations, which are used for numerical weather prediction, have solutions covering a broad frequency spectrum. The low-frequency rotational components are of major meteorological significance, while the high-frequency gravity wave components are normally of minor importance and are generally regarded as noise. The atmosphere maintains itself in a state of near balance such that high-frequency motions have small amplitudes. It is important to mirror this balance in numerical simulations if spurious or anomalous effects are to be avoided.

The integration techniques developed in this paper are designed to separate the low- and high-frequency components of the flow to simulate the former accurately and to eliminate the latter. The methods, which are based on the Laplace and Z transforms, derive from the idea of nonlinear normal mode initialization (NNMI). In NNMI the amplitudes of the gravity wave components of the initial data are modified in such a way that their initial tendencies vanish. This is achieved by an iterative process (for a review of NNMI and further references see Daley 1981). Provided the integration proceeds undisturbed, the amplitudes of these components remain small, at least in the short and medium range. If the model state is perturbed during the simulation, anomalously large gravity-wave oscil-

lations will be generated unless a balance is imposed by reinitialization.

The Laplace transform filtering integration technique automatically achieves such a balance. Each step of the method corresponds to a forward model time step and simultaneously a single iteration of NNMI. The method ensures a noise-free simulation by continuously maintaining the model in a quasi-balanced state. If this state is disturbed during the integration, for example by data insertion, balance is quickly restored by the scheme. Thus, a model that uses the scheme is shockproof in the sense that it can respond to changes in its state during the course of the integration without suffering data shock. The scheme can thus be used for insertion of asynoptic observations and is of interest in the context of continuous data assimilation.

The use of the Laplace transform (LT) for filtering is described in section 2, and a filtering integration scheme based on it is developed. In section 3 this scheme is applied to the shallow-water equations. In section 4 a forecast using the LT technique is compared to a forecast with a more conventional scheme, and it is shown that the technique is capable of accurately simulating an atmospheric flow. In section 5 a number of perturbation experiments are described. The LT model is shown to be able to absorb and adjust to perturbations without problems. By comparison, a model using a conventional integration scheme suffers data shock and responds noisily to perturbations. These results demonstrate the potential of the LT filtering scheme for continuous data assimilation. An alterna-

Corresponding author address: Dr. Peter Lynch, Irish Meteorological Service, Glasnevin Hill, Dublin 9, Ireland.

tive formulation of the filtering integration scheme based on the Z transform (ZT) is described in section 6, and compared to the LT scheme.

The filtering capabilities of the Laplace transform were first employed by Lynch (1985a) in an initialization scheme, and the method was applied to initialize data for a barotropic model (Lynch 1985b). Lynch later applied it to a limited area version of the ECMWF baroclinic gridpoint model with results (unpublished) very similar to an NNMI method.

An integration technique using the LT was described in Van Isacker and Struylaert (1985). They applied it to a one-dimensional model and to a spectral model with low-order (T19) truncation. Further discussion of the results for the baroclinic case is found in Van Isacker and Struylaert (1986). The authors report there that the method allows a long time step without loss of accuracy. An application of a similar method to a simple one-dimensional model is described in Lynch (1986) and its relevance for data assimilation is discussed.

Daley (1980) described an integration method in which the low-frequency rotational Hough modes are forecast while the high-frequency gravity modes are diagnosed at each time step. The LT method is similar to this scheme, but the distinction between low and high frequencies is made implicitly. A comparison between the Daley scheme and the LT method is being made and the results will be published elsewhere.

2. Theoretical basis of the Laplace transform scheme

The use of the LT for filtering is reviewed and the method is used to derive a scheme for the solution of a general nonlinear equation. The description below is brief; further details may be found in Lynch (1985a,b; 1986). The general theory of LT is presented in Doetsch (1971).

a. Filtering by modification of the inverse transform

Consider a function $f(t)$ with components of various frequencies

$$f(t) = \sum_{k=1}^{K} a_k \exp(i\omega_k t). \qquad (2.1)$$

The LT of f is a meromorphic function of s:

$$\hat{f}(s) \equiv \mathfrak{L}\{f\} = \sum_{k=1}^{K} a_k/(s - i\omega_k) \qquad (2.2)$$

with poles on the imaginary axis of the s plane. The original function is recovered by means of the inverse transform

$$f(t) = \mathfrak{L}^{-1}\{\hat{f}\} \equiv \frac{1}{2\pi i} \int_C e^{st}\hat{f}(s)ds \qquad (2.3)$$

where the contour C is a line parallel to the imaginary axis and to the right of all singularities of $\hat{f}$ (Doetsch 1971, chapter 6).

The components of $f(t)$ with frequencies below some cutoff value γ may be isolated by modifying the inversion integral: the contour C is replaced by a circle C* of radius γ (see Fig. 1)

$$f^*(t) = \mathfrak{L}^*\{\hat{f}\} \equiv \frac{1}{2\pi i} \oint_{C^*} e^{st}\hat{f}(s)ds. \qquad (2.4)$$

The function f^* is just the sum of the components resulting from those poles of $\hat{f}$ which fall within C*, namely the components with frequencies less than γ. Thus, the operator $\mathfrak{L}^*\mathfrak{L}$ acts as an *ideal low-pass filter* with cutoff frequency γ.

In practice the integral (2.4) must be evaluated numerically. The circle C* is approximated by a circumscribed N-gon C_N^* (Fig. 2), and the integrand is calculated at the midpoints s_n of the edges of C_N^*. The discrete modified inverse LT is then defined as

$$\mathfrak{L}_N^*\{\hat{f}\} = \frac{(1/\kappa)}{2\pi i} \sum_{n=1}^{N} \hat{f}(s_n)e^{s_n t}\Delta s_n. \qquad (2.5)$$

[The correction factor $\kappa = \tan(\pi/N)(\pi/N)^{-1}$ ensures that the inversion is exact for $\hat{f}(s) = c/s$, the transform of a constant c.] Using the fact that $\Delta s_n/s_n = 2\pi i\kappa/N$ this transform can be rewritten as
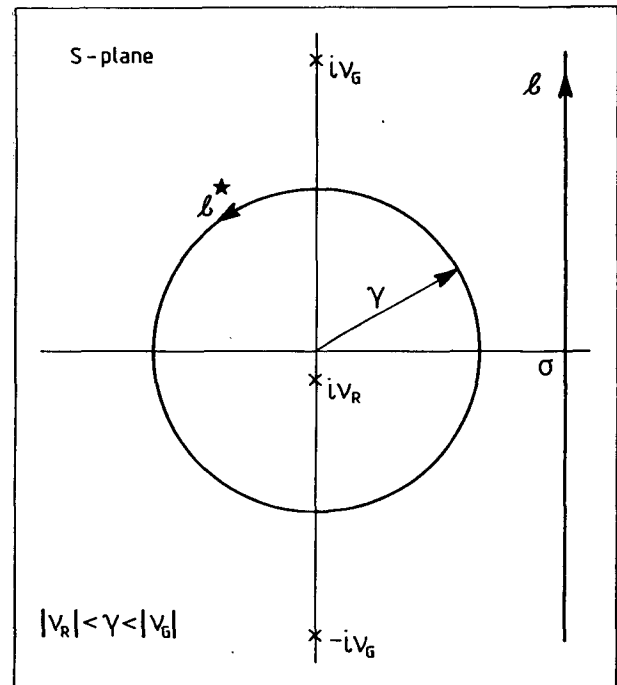

FIG. 1. Contours in the s plane used for the regular and modified inverse Laplace transform. The value of γ is chosen to separate the rotational frequencies (ν_R) and the gravity-wave frequencies (ν_G).
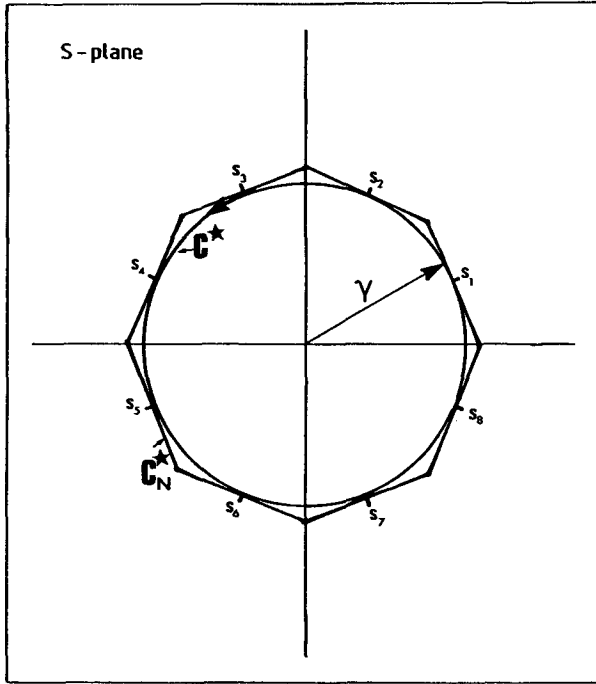
FIG. 2. Contour C^* used to define the modified operator $\tilde{\mathfrak{L}}^*$, and circumscribed polygon C_N^* used in approximating the contour integral by a finite sum $\mathfrak{L}_N^*$.

$$\mathfrak{L}_N^*\{\hat{f}\} = \frac{1}{N}\sum_{n=1}^{N}\hat{f}(s_n)e^{s_n t}s_n. \qquad (2.6)$$

In practice it has been found that $N = 8$, as in Fig. 2, leads to completely satisfactory results. Normally, this would require the evaluation of $\hat{f}(s)$ at eight points. However, when the original function $f(t)$ is real it is easy to show that

$$\frac{1}{2\pi i}\oint_{C^*}e^{st}\hat{f}(s)ds = \frac{1}{\pi}\int_{C^+}\text{Im}[e^{st}\hat{f}(s)ds] \qquad (2.7)$$

where Im[ ] is the imaginary part and C^+ is the upper half of C^*. This halves the necessary work, as only four evaluations of $\hat{f}$ are required to calculate the integral on the right-hand side.

The numerical operator $\mathfrak{L}_N^*\mathfrak{L}$ is no longer an ideal low-pass filter. Its effect on components of varying frequencies has been investigated by Van Isacker and Struylaert (1985). They proposed that the exponential factor in (2.6) be replaced by its Taylor series truncated to N terms:

$$e^{s_n t} \rightarrow e_N{}^{s_n t} \equiv \sum_{k=0}^{N-1}\frac{(s_n t)^k}{k!}.$$

The operator $\mathfrak{L}_N^*$ thus modified will be denoted by $\tilde{\mathfrak{L}}_N^*$. This approximation allowed Van Isacker and Struylaert to find an expression for the response, and

they showed that the effect of the modified operator was as follows:

$$\tilde{\mathfrak{L}}_N^*\mathfrak{L}\{e^{i\omega t}\} = M_N(\omega)e_N{}^{i\omega t} \qquad (2.8)$$

where the "response function" is given by

$$M_N(\omega) = [1 + (i\omega/\gamma)^N]^{-1}.$$

For N a multiple of 4 this is the square of the response of a Butterworth filter (Hamming 1989), and approximates a step function with a corner point at $\omega = \gamma$. It is real in this case implying that no phase error is incurred.

b. Application to the solution of a nonlinear system

Consider a system whose state at time t is specified by the vector $\mathbf{X}(t)$, which is governed by an equation of the form

$$\frac{d\mathbf{X}}{dt} + \mathbf{LX} + \mathbf{N}(\mathbf{X}) = 0, \qquad (2.9)$$

where $\mathbf{L}$ is a linear operator and $\mathbf{N}$ a nonlinear vector function. If the system is in the state $\mathbf{X}^0$ at time $t = 0$ then the LT of this equation is

$$\mathbf{M}\hat{\mathbf{X}} + \hat{\mathbf{N}} = \mathbf{X}^0 \qquad (2.10)$$

where $\mathbf{M}(s) = (s\mathbf{I} + \mathbf{L})$ with $\mathbf{I}$ the identity matrix.

If one considers the evolution of the system over a short time interval $(0, \Delta t)$, and assumes that the nonlinear term does not vary, then (2.10) may be solved as follows

$$\hat{\mathbf{X}} = \mathbf{M}^{-1}[\mathbf{X}^0 - \mathbf{N}^0/s] \qquad (2.11)$$

where $\mathbf{N}^0 = \mathbf{N}(\mathbf{X}^0)$. Then, to find the solution at time $t = \Delta t$ the inverse LT is applied

$$\mathbf{X}(\Delta t) = \mathfrak{L}^{-1}\{\mathbf{M}^{-1}[\mathbf{X}^0 - \mathbf{N}^0/s]\}|_{t=\Delta t}.$$

If we are interested only in the slowly varying components of the flow we may replace $\mathfrak{L}^{-1}$ by the modified inverse $\mathfrak{L}^*$ which acts to filter out the high-frequency components:

$$\mathbf{X}^1 = \mathbf{X}^*(\Delta t)$$
$$= \mathfrak{L}^*\{\mathbf{M}^{-1}[\mathbf{X}^0 - \mathbf{N}^0/s]\}|_{t=\Delta t}. \qquad (2.12)$$

Having the solution at $t = \Delta t$ one may proceed stepwise to extend the forecast: the solution is advanced from $n\Delta t$ to $(n + 1)\Delta t$ by

$$\mathbf{X}^{n+1} = \mathfrak{L}^*\{\mathbf{M}^{-1}[\mathbf{X}^n - \mathbf{N}^n/s]\}|_{t=\Delta t}. \qquad (2.13)$$

Alternatively, a leapfrog time-stepping scheme may be used:

$$\mathbf{X}^{n+1} = \mathfrak{L}^*\{\mathbf{M}^{-1}[\mathbf{X}^{n-1} - \mathbf{N}^n/s]\}|_{t=2\Delta t}. \qquad (2.14)$$

Here the origin of time for the transform is $(n - 1)\Delta t$, so that $\mathbf{X}^{n-1}$ is the "initial condition," and the nonlinear terms are evaluated at the center of the interval [$(n$

$-1)\Delta t$, $(n + 1)\Delta t]$. Clearly, numerous other formulations of the time stepping algorithm are possible.

3. Application to a shallow-water model

The LT integration method will now be applied in the context of a model based on the shallow-water equations. The advection terms will be discretized in a manner based on the semi-Lagrangian approach, which yields attractive stability characteristics and enables a large time step to be used.

The shallow-water equations may be written as follows

$$\frac{\partial u}{\partial t} + \mathbf{V} \cdot \nabla u - f_0 v + \Phi_x + N_u = 0 \quad (3.1)$$

$$\frac{\partial v}{\partial t} + \mathbf{V} \cdot \nabla v + f_0 u + \Phi_y + N_v = 0 \quad (3.2)$$

$$\frac{\partial \Phi}{\partial t} + \mathbf{V} \cdot \nabla \Phi + \bar{\Phi} \nabla \cdot \mathbf{V} + N_\Phi = 0 \quad (3.3)$$

where the notation is conventional. The Coriolis parameter has been given a mean value f_0, and variations from this are included in the nonlinear terms:

$$N_u = -[(f - f_0) + (u \tan\phi)/a]v$$

$$N_v = +[(f - f_0) + (u \tan\phi)/a]u$$

$$N_\Phi = (\Phi - \bar{\Phi})\nabla \cdot \mathbf{V}.$$

These equations will be used in the following to make a forecast over a limited domain.

When the semi-Lagrangian scheme is used for integration of the advection processes, the total time derivative is approximated by

$$\frac{du}{dt} \approx \frac{(u_G^{n+1} - u_*^n)}{\Delta t}$$

which involves the change in value of u along a trajectory. The value at the arrival grid point G at time ($n + 1)\Delta t$ is u_G^{n+1}, and u_*^n is the (interpolated) value at the departure point on the trajectory at time $n\Delta t$. This may also be written as

$$\frac{du}{dt} \approx \left(\frac{u_G^{n+1} - u_G^n}{\Delta t}\right) + \left(\frac{u_G^n - u_*^n}{\Delta t}\right). \quad (3.4)$$

Clearly, the first term on the right-hand side approximates the local (Eulerian) time derivative at grid point G; thus the second term is an approximation to the advection, for example

$$(\mathbf{V} \cdot \nabla u)^n \approx \left(\frac{u_G^n - u_*^n}{\Delta t}\right) \equiv A_u^n. \quad (3.5)$$

Use of this form of discretizing the advection ensures that the numerical domain of dependence surrounds the trajectory. It is a necessary condition for stability of a numerical scheme that the physical domain of

dependence should be encompassed by the numerical domain of dependence. It will be seen from the integration results below that the use of (3.5) leads to a stable scheme, unrestricted by any CFL criterion.

The LT will be applied to the time-continuous form of the equations, that is to (3.1), (3.2), (3.3). However, in order to avail of the attractive stability properties of the semi-Lagrangian approach, the advection terms will first be discretized using (3.5). The transforms of the equations may then be written as follows

$$s\hat{u} - f_0\hat{v} + \hat{\Phi}_x = u^n - (A_u^n + N_u^n)/s \equiv R_u \quad (3.6)$$

$$s\hat{v} + f_0\hat{u} + \hat{\Phi}_y = v^n - (A_v^n + N_v^n)/s \equiv R_v \quad (3.7)$$

$$s\hat{\Phi} + \bar{\Phi}(\nabla \cdot \hat{\mathbf{V}}) = \Phi^n - (A_\Phi^n + N_\Phi^n)/s \equiv R_\Phi. \quad (3.8)$$

The origin of time for the transformation is $t = n\Delta t$, and the advection and other nonlinear terms have been approximated by their values at this time. For a given value of s the right-hand sides may be calculated, and the system solved for $(\hat{u}, \hat{v}, \hat{\Phi})$ as functions of s. Equations (3.6) and (3.7) may be solved for $\hat{u}$ and $\hat{v}$ in turn

$$(s^2 + f_0^2)\hat{u} = -(s\hat{\Phi}_x + f_0\hat{\Phi}_y) + [R_u^n + (s/f_0)R_v^n] \quad (3.9)$$

$$(s^2 + f_0^2)\hat{v} = -(s\hat{\Phi}_y - f_0\hat{\Phi}_x) + [R_v^n - (s/f_0)R_u^n]. \quad (3.10)$$

If these relations are used to eliminate the divergence term in (3.8), a Helmholtz equation is immediately obtained for $\hat{\Phi}$:

$$\left[\nabla^2 - \left(\frac{s^2 + f_0^2}{\bar{\Phi}}\right)\right]\hat{\Phi} = F_\Phi \quad (3.11)$$

where the right-hand forcing function is given by

$$F_\Phi = \left[\frac{1}{s}\nabla \cdot (\mathbf{R_v}) - \left(\frac{s^2 + f_0^2}{s\bar{\Phi}}\right)(\Phi^0 - N_\Phi/s)\right] \quad (3.12)$$

with $\mathbf{R_v}$ representing the vector (R_u, R_v).

Equation (3.11) is particularly simple in having constant coefficients. This is a result of separating the Coriolis parameter into mean and variable parts and including the latter with the nonlinear terms. This Helmholtz equation may be solved using a fast elliptic solver. The subroutine HWSSSP, developed at NCAR (Swarztrauber and Sweet 1975) was modified to cover the case of complex variables.

If the quantity $Q = (s^2 + f_0^2)/\bar{\Phi}$ is equal to an eigenvalue $-\lambda_n^2$ of the Laplacian operator for the domain and boundary conditions used, the solution of (3.11) is not unique. This would occur if the cutoff frequency had the value $\gamma = (\bar{\Phi}\lambda_n^2 + f_0^2)^{1/2}$ for some n, and such values should be avoided in choosing γ. In practice, no difficulty has been experienced in solving (3.11).

A model based on the previously transformed equations has been written and used to prepare a number

of forecasts. The advection terms, such as (3.5) are calculated using bicubic interpolation with the upstream point estimated using the method of McDonald and Bates (1987). If (u, v, Φ) are known at time $n\Delta t$, the forcing term (3.12) can be calculated and the Eq. (3.11) solved for $\dot{\Phi}$. Then $\hat{u}$ and $\hat{v}$ are obtained from (3.9) and (3.10). This step is repeated four times, with values of s at the center of each upper edge of the octogon in Fig. 2. The inversion operator may now be applied using (2.6) and (2.7) with $t = \Delta t$, to obtain (u, v, Φ) at time ($n + 1$)Δt. Due to the filtering properties of the operator, only the low-frequency components will be contained in the solution. The radius γ of the contour C^* is chosen to correspond to a cutoff period of 6 h: $\gamma = 2\pi/6.60^2 = 0.00029$ s^{-1}. Forecast results using this model are described in the following section.

4. Comparison with a conventional scheme

To investigate the accuracy of the LT scheme, a series of parallel runs using this method and a more conventional scheme were completed. The two models are denoted SALT (stable advection Laplace transform) and SLSI (semi-Lagrangian semi-implicit). The former uses the time integration scheme described in section 3. The latter is a one-level version of the model described by McDonald (1986), which is used in operational practice at the Irish Meteorological Service. The integration domain is identical for the two models; the area, which can be seen by reference to Fig. 3, is covered by a 2° × 2° C grid of 40 × 26 points. The geopotential and normal wind are held constant along the boundaries.

The initial data is the operational 500-hPa analysis valid at 0000 UTC 22 November 1982, and initialized using the LT technique (Lynch 1985b). This is shown in Fig. 3. In the initialization the nonlinear terms were calculated using the model SALT with a single time step for each iteration. The time step chosen was Δt = 600 s. However, when a time step of 1200 s was used the results were virtually identical: the initialized height fields in the two cases differed by less than a meter (with rms difference 0.14 m).

The 24-h forecast made using SLSI with a time step of 600 s is shown in Fig. 4. This is used as the reference forecast. The corresponding forecast made using the LT model SALT with the same time step is very similar. The difference between the two forecasts is shown in Fig. 5. The maximum difference in the height field is 21 m, and the rms difference is 4.09 m. The maximum and rms differences in the wind fields are 2.3 m s^{-1} and 0.64 m s^{-1}, respectively. The small values of these differences between the two forecasts indicate that the Laplace transform model is faithfully simulating the flow. The differences are, for practical purposes, negligible.

The great advantage of using a semi-Lagrangian formulation of advection is that relatively large time steps may be used without significant loss of accuracy and without the onset of instability. A forecast using SLSI with a 1-h time step was made and compared to that with a 600-s time step. The rms differences in height and wind were 2.66 m and 0.45 m s^{-1}. These time truncation errors are very small, and show that an accurate forecast is obtained using the reference model with a 1-h time step.
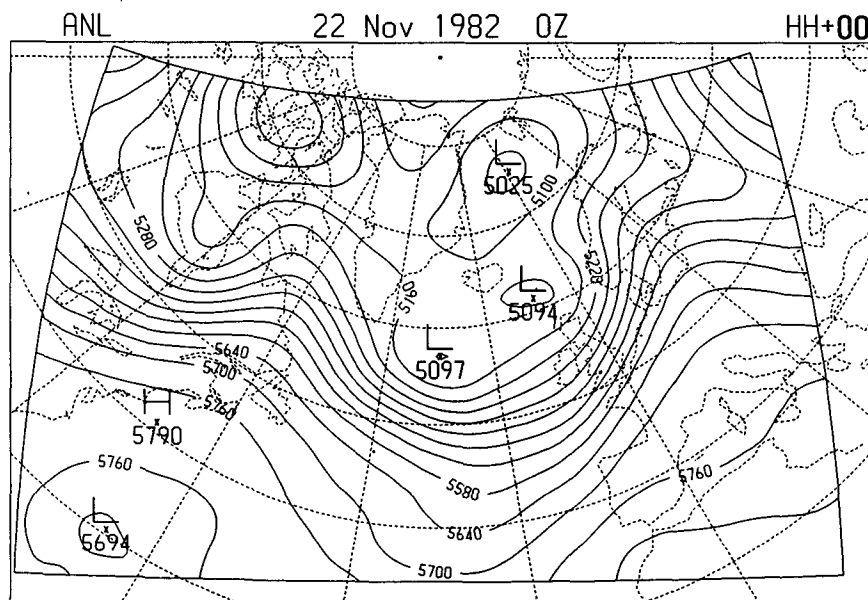

FIG. 3. Initial geopotential height field: 500-hPa analysis
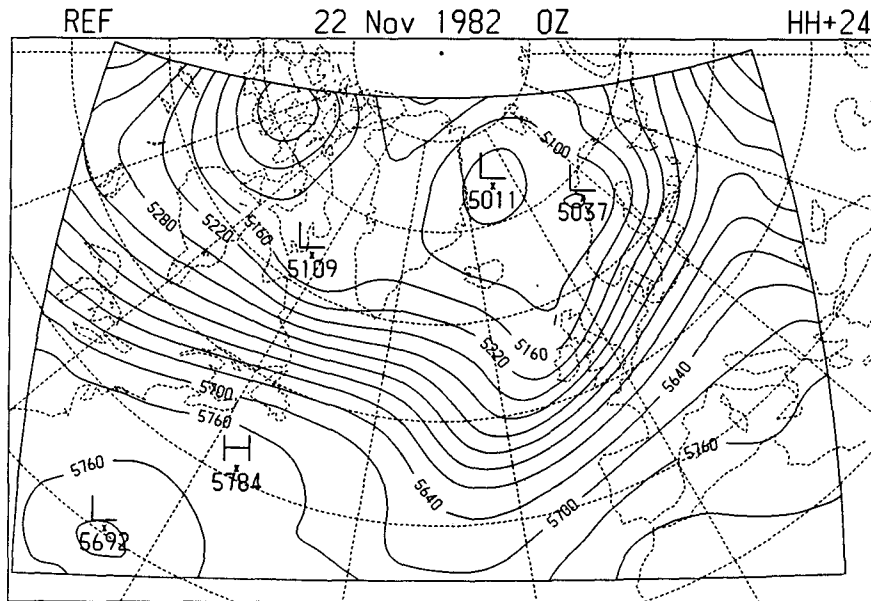valid at 0000 UTC 22 November 1982.

FIG. 4. The 24-h forecast of geopotential height made with the reference model SLSI.

The LT model SALT was also run with $\Delta t = 1$ h, and compared to the SALT forecast with $\Delta t = 600$ s. The rms differences in height and wind were 6.82 m and 1.37 m s^{-1}. These time truncation errors are significantly larger than those for the reference model SLSI. The errors in the SALT forecast with $\Delta t = 1$ h, as measured against the reference SLSI with $\Delta t = 600$ s, were 10.5 m rms for height and 1.85 m s^{-1} for wind. Thus, although the integration with SALT remains stable for large time steps, there is an evident loss of accuracy as the time step is increased. The error in SLSI is quadratic in Δt; for SALT the error grows linearly with the time step. Although the SALT and SLSI forecasts with $\Delta t = 1$ h did not differ greatly (the maximum height difference was 58 m and the two maps of geopotential looked very similar), the differences were larger than would be desirable in an operational context. Thus, despite the attractive stability properties
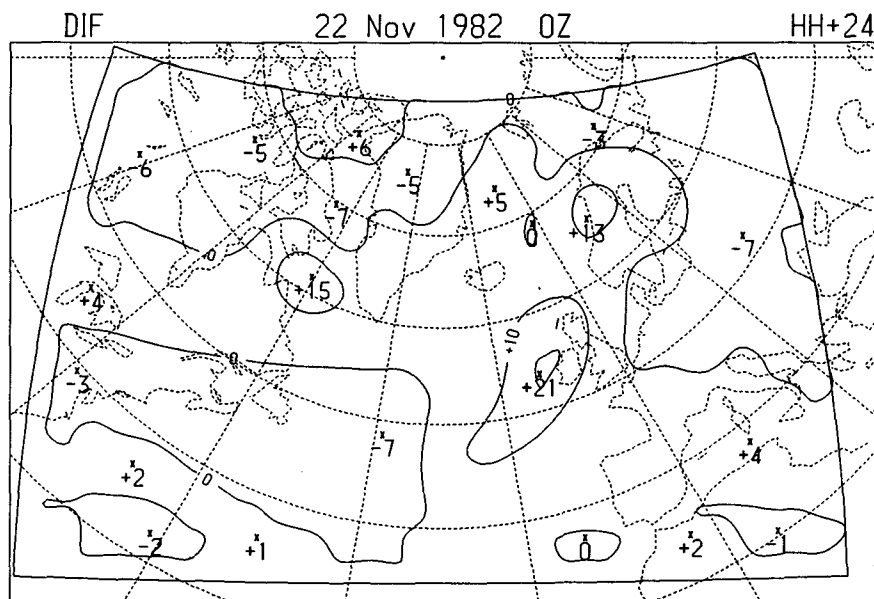

FIG. 5. Height difference between the 24-h forecasts made
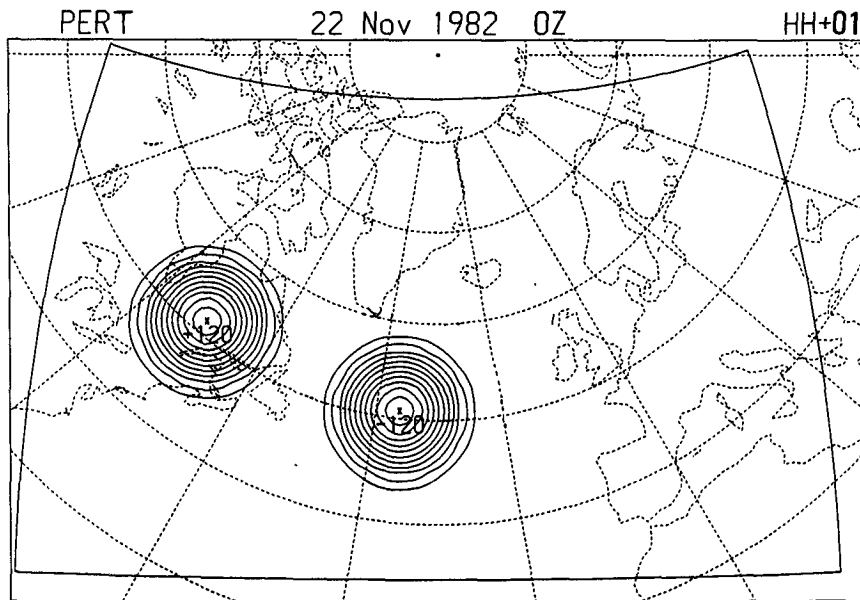with the two models SALT and SLSI.

PERT   22 Nov 1982   0Z   HH+01

FIG. 6. Perturbation height field added to the height forecasts 1 h after the initial time.

of the LT scheme for large Δt, it is unlikely to be of sufficient accuracy for large time steps, as it is currently formulated. Thus far there has been no success in devising an advection scheme combined with the LT technique, which has a quadratic time truncation error.

5. Perturbation experiments

A number of approaches have been made to the problem of assimilation of asynoptic data. The technique most in vogue at present is four-dimensional variational assimilation using the adjoint model equations. This appears very promising for the future, but is computationally very expensive. In the following, the simple ploy of inserting data at its time of validity is considered, and the response of a model to inserted data is investigated.

One of the attractive features of the LT integration technique is its ability to remove data shock by rapid adjustment to changes induced by the insertion of data during a forecast. This shockproof character of the SALT model will be demonstrated by some perturbation experiments.

Figure 6 depicts a geopotential perturbation comprising a low centered at grid point (19, 9) and a high at point (9, 13), both with magnitude 120 m. The spatial distribution of each component is given by

$$\Phi(r) = \begin{cases} \Phi_0[1 - (r/R)^2]^3, & r < R \\ 0, & r \geq R \end{cases}$$

where $|\Phi_0/g| = 120$ m, r is the distance from the central point and R determines the scale. The perturbations in Fig. 6 have a scale of $R = 5\Delta x = 1000$ km.

The high and low perturbations are added to the forecast fields 1 h after the initial time. They may be thought to represent the influences of observations at the center points indicating geopotential heights 120 m above and below the forecast values. At the same time, the wind field is modified by the addition of a geostrophic flow corresponding to the height perturbation. Since the geostrophic relationship is linear, the addition of these height and wind perturbations will preserve geostrophic balance if such exists prior to the data insertion. Of course, the balance in the atmosphere is more subtle, which makes the assimilation of data so tricky.

The Rossby radius of deformation is defined by $L_R^2 = \bar{\Phi}/f_0^2$. With a mean depth of 5500 m and $f_0 = 10^{-4}$ s^{-1} it has a value of approximately 2500 km. Since the scale R of the imposed disturbance is considerably less that this, the perturbation may be regarded as small. According to geostrophic adjustment theory, the wind perturbation should predominate with the height field tending to adjust to the new wind field.

The two models SLSI and SALT were run in parallel, both perturbed in the same way at HH + 01 (i.e., one hour after the initial time), and the ensuing forecasts compared. The maximum positive and negative differences between the perturbed and unperturbed forecasts were calculated every hour for each model. These differences effectively measure how the amplitudes of the high and low perturbations evolve in time. They are shown in Fig. 7. For both models the high weakens and the low intensifies. This is consistent with adjustment theory: for cyclonic flow the geostrophic wind exceeds the gradient wind; so, if the wind perturbation is assimilated the low must deepen to maintain gradient
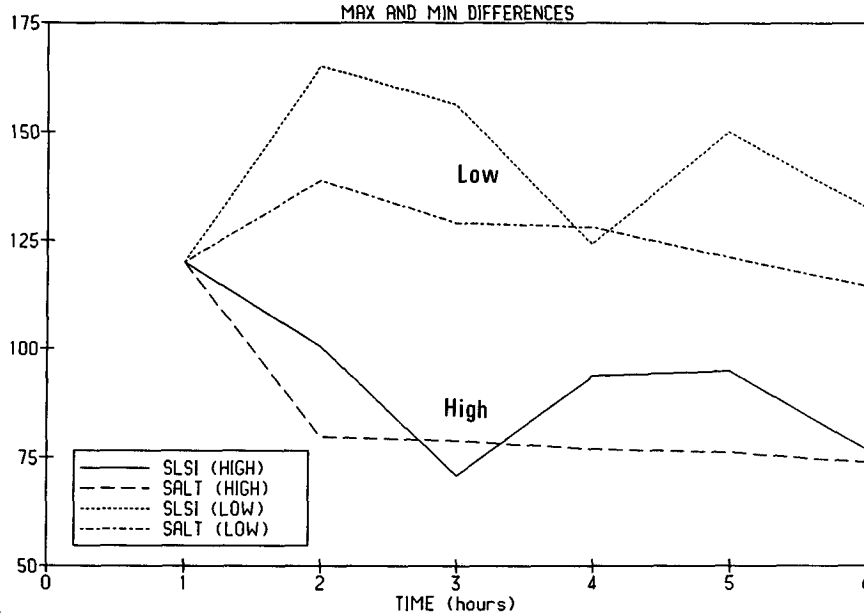
FIG. 7. Absolute values of the maximum positive (High) and negative (Low) differences
between the perturbed and unperturbed forecasts for SLSI and SALT.

balance. By a similar argument the high must weaken. This behavior is found for both models.

The character of the response to the perturbation differs for the two models. The LT model appears to adjust rapidly to the inserted data, with the evolution being smooth after HH + 02. For SLSI, the amplitudes of the high and low continue to oscillate for several hours (Fig. 7). This is confirmed by a plot of the di-

vergence at grid point (19, 9), where the low is originally inserted (see Fig. 8). For SLSI the perturbation elicits a noisy response which persists for over 6 h, being gradually attenuated by a light divergence damping (dashed line, Fig. 8). No such noise is experienced by the model SALT (dot–dashed line, Fig. 8).

The ability of the LT model to assimilate a perturbation without data shock or subsequent noise is an
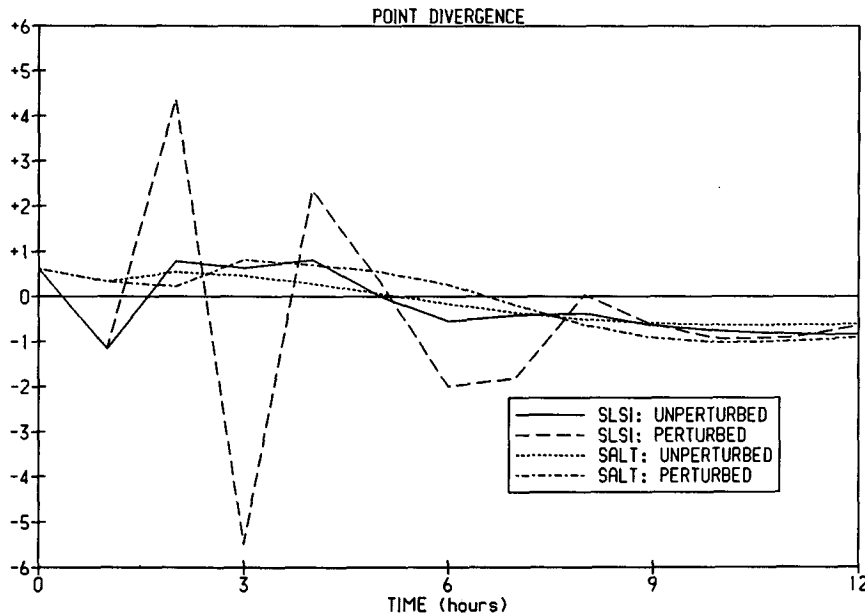

FIG. 8. Evolution of the divergence at grid point (19, 9) for the unperturbed
and perturbed forecasts using the two models.

(a)REF   22 Nov 1982 0Z   HH+24
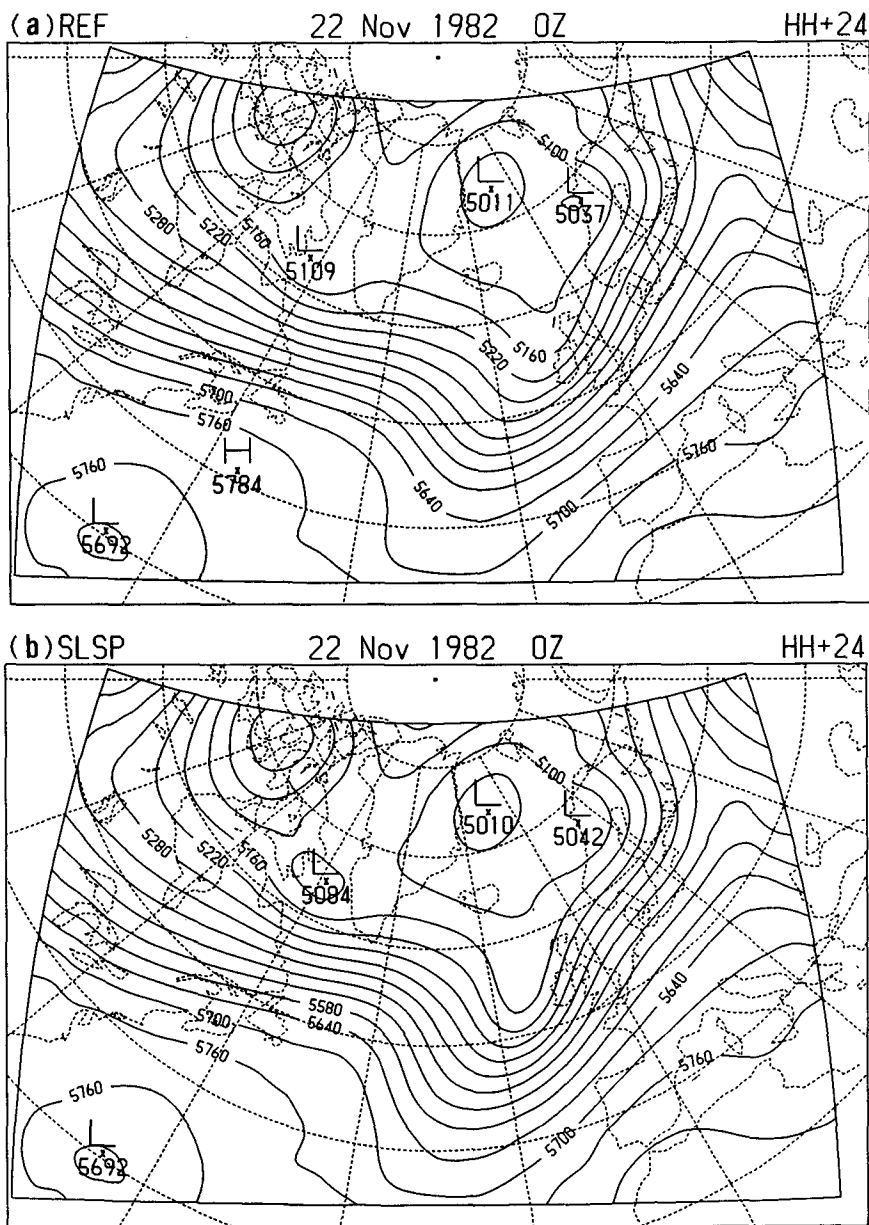
(b)SLSP   22 Nov 1982 0Z   HH+24

FIG. 9. (a) Unperturbed 24-h height forecast with SLSI.
(b) Perturbed 24-h height forecast with SLSI.

attractive feature of this integration scheme. If data is to be inserted hour by hour, noise from the earlier insertions may interfere with quality control and assimilation of the later ones. The model SLSI obviously suffers in this respect. The model SALT is, in this sense, shockproof.

The ultimate effect of the perturbations is seen by comparing Figs. 9a,b. These are, respectively, the unperturbed and perturbed 24-h forecasts made using SLSI. The main effects of the inserted data are the sharpening of the trough to the west of Ireland and the intensification of the ridge over the North Sea. The forecasts made with SALT look very similar to the cor-

responding SLSI forecasts. The differences between the perturbed and unperturbed forecasts for both models are shown in Fig. 10. It can be seen that the long-term consequences of the perturbations are very similar for the two models. It is the short-term response that is markedly different.

6. An alternative scheme based on the Z transform

a. Formulation of the scheme

If the equations of motion are discretized in time, the resulting finite difference system is no longer amenable to the LT approach. Instead, the discrete ana-

logue of this technique, the Z transform, becomes applicable.

The definition and principal properties of the Z transform are given in the Appendix. It is shown there that an operator $\mathfrak{Z}^*\mathfrak{Z}$, similar to $\mathfrak{L}^*\mathfrak{L}$, acts as an ideal low-pass filter on a discrete sequence comprising components of various frequencies. A numerical integration scheme based on this filter can be developed in a manner completely analogous to the scheme based on the modified inverse LT as described in section 3.

The starting point is as before the shallow-water system (3.1)–(3.3). These equations are discretized in time by considering changes along a trajectory ending at grid point G at time $(n + 1)\Delta t$ and departing at time $n\Delta t$ from a point denoted by an asterisk. As before, the Lagrangian derivative is split into two parts, for example

$$\frac{du}{dt} \approx \left(\frac{u_G^{n+1} - u_G^n}{\Delta t}\right) + \frac{A^n(u)}{\Delta t}$$

where the advection operator $A^n(\;\;)$ is defined by
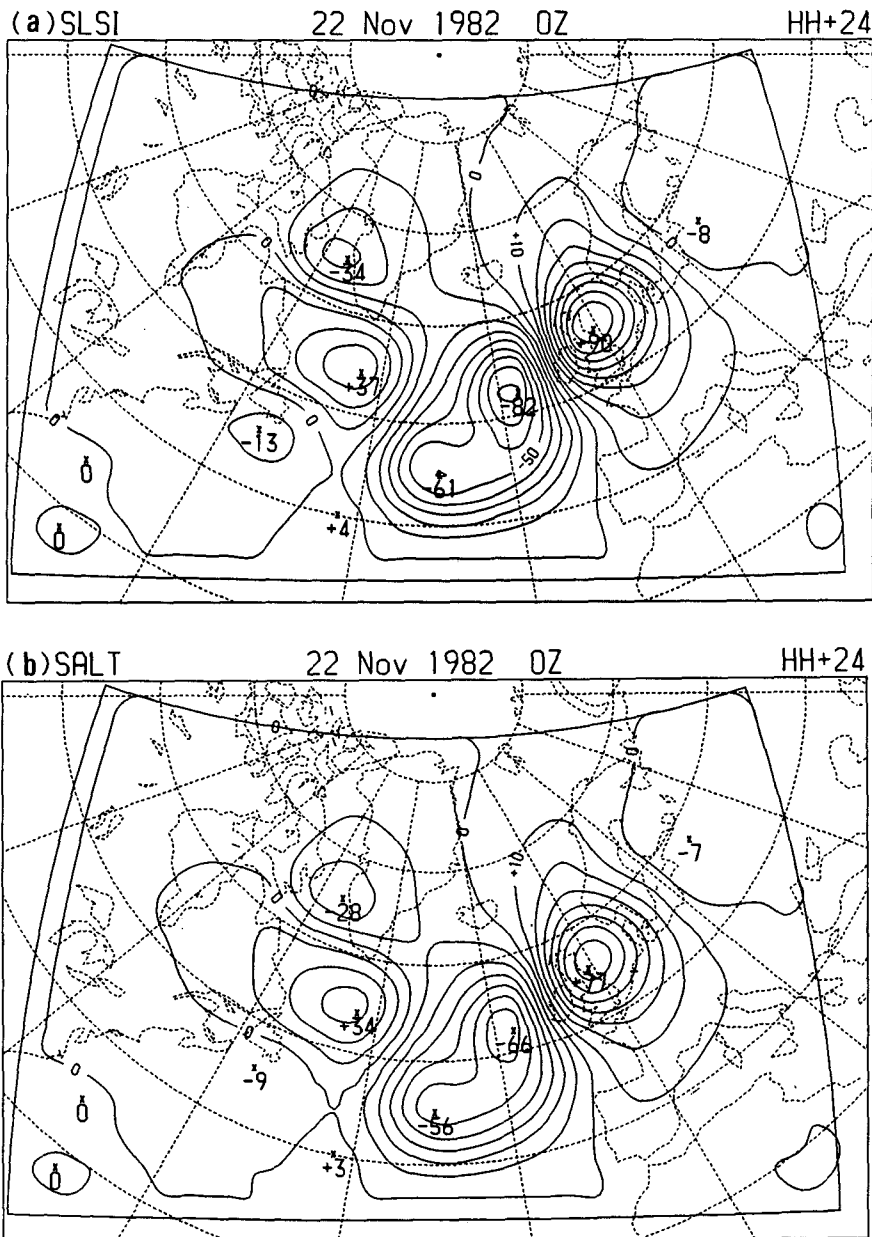
$$A^n(u) \equiv (u_G^n - u_*^n)$$

FIG. 10. (a) Difference between the perturbed and unperturbed height forecasts with SLSI. (b) Corresponding difference for the model SALT.

[compare (3.4) and (3.5)]. In a similar manner, averages along the trajectory are split into two parts as follows:

$$f_0 u \approx (1/2)f_0[(u_G{}^{n+1} + u_G{}^n) - A^n(u)].$$

The discretized shallow-water equations may now be written as follows:

$$(u^{n+1} - u^n) - F(v^{n+1} + v^n)$$
$$+ D(\Phi_x{}^{n+1} + \Phi_x{}^n) + B_u{}^n = 0 \quad (6.1)$$

$$(v^{n+1} - v^n) + F(u^{n+1} + u^n)$$
$$+ D(\Phi_y{}^{n+1} + \Phi_y{}^n) + B_v{}^n = 0 \quad (6.2)$$

$$(\Phi^{n+1} - \Phi^n) + \bar{\Phi}D(\nabla \cdot \mathbf{V}^{n+1} + \nabla \cdot \mathbf{V}^n) + B_\Phi{}^n = 0. \quad (6.3)$$

Here $F = f_0 \Delta t / 2$, $D = \Delta t / 2$ and the advection, and other nonlinear terms have been combined:

$$B_u{}^n = A^n(u + Fv - D\Phi_x) + \Delta t(N_u{}^n)_*$$

$$B_v{}^n = A^n(v - Fu - D\Phi_y) + \Delta t(N_v{}^n)_*$$

$$B_\Phi{}^n = A^n(\Phi - \bar{\Phi}D\nabla \cdot \mathbf{V}) + \Delta t(N_\Phi{}^n)_*.$$

The A terms involve difference at time $n\Delta t$ between the arrival and departure points; the N terms are evaluated at the departure point; all remaining terms in (6.1)–(6.3) are calculated at the arrival grid point G.

Equations (6.1)–(6.3) are now Z-transformed, taking the origin of time at $n\Delta t$ and using (A.3). The Z transform of u is denoted by $\check{u}$, etc. The B terms are evaluated at time $n\Delta t$ and assumed to be constant. This results in:

$$[(z - 1)\check{u} - zu^n] - F[(z + 1)\check{v} - zv^n]$$
$$+ D[(z + 1)\check{\Phi}_x - z\Phi_x{}^n] + \left(\frac{z}{z-1}\right)B_u{}^n = 0$$

$$[(z - 1)\check{v} - zv^n] + F[(z + 1)\check{u} - zu^n]$$
$$+ D[(z + 1)\check{\Phi}_y - z\Phi_y{}^n] + \left(\frac{z}{z-1}\right)B_v{}^n = 0$$

$$[(z - 1)\check{\Phi} - z\Phi^n] + \bar{\Phi}D[(z + 1)\nabla \cdot \check{\mathbf{V}} - z\nabla \cdot \mathbf{V}^n]$$
$$+ \left(\frac{z}{z-1}\right)B_\Phi{}^n = 0.$$

Defining $\zeta = (z + 1)/(z - 1)$, the three equations may be written in the form

$$\check{u} - F\zeta\check{v} + D\zeta\check{\Phi}_x = R_u \quad (6.4)$$

$$\check{v} + F\zeta\check{u} + D\zeta\check{\Phi}_y = R_v \quad (6.5)$$

$$\check{\Phi} + \bar{\Phi}D\zeta(\nabla \cdot \check{\mathbf{V}}) = R_\Phi \quad (6.6)$$

where the right-hand sides are functions of z and of the variables (u, v, Φ) at time $n\Delta t$. These equations are formally similar to (3.6)–(3.8) and the procedures are as before. Equations (6.4) and (6.5) are solved for $\check{u}$ and $\check{v}$ in terms of $\check{\Phi}$:

$$(1 + F^2\zeta^2)\check{u} = -D\zeta(\check{\Phi}_x + F\zeta\check{\Phi}_y) + (R_u + F\zeta R_v) \quad (6.7)$$

$$(1 + F^2\zeta^2)\check{v} = -D\zeta(\check{\Phi}_y - F\zeta\check{\Phi}_x) + (R_v - F\zeta R_u). \quad (6.8)$$

These expressions are used to eliminate the divergence term in (6.6), yielding a Helmholtz equation for $\check{\Phi}$:

$$\left[\nabla^2 - \left(\frac{1 + F^2\zeta^2}{D^2\zeta^2\bar{\Phi}}\right)\right]\check{\Phi} = F_\Phi \quad (6.9)$$

where the right-hand forcing function may be calculated for a specified z from known quantities.

The solution is essentially the same as described in section 3. Let (u, v, Φ) be known at time $n\Delta t$; the forcing term of (6.9) can then be calculated and the equation solved for $\check{\Phi}$. Then $\check{u}$ and $\check{v}$ are obtained from (6.7) and (6.8). This step is repeated four times, with $z_n = \exp(s_n\Delta t)$, where s_n is the value of s at the center of each upper edge of the octogon in Fig. 2. The inversion operator may now be applied, using (A.6) with $t = \Delta t$, to obtain (u, v, Φ) at time $(n + 1)\Delta t$. The same sequence of operations may now be repeated as often as necessary to reach the required forecast time. As a result of the filtering properties of the modified inversion operator, the solution will contain only low-frequency components. The radius γ of the contour C_s^* is chosen once again to correspond to a cutoff period of 6 h.

b. Comparison of the Laplace and Z transform schemes

A series of forecasts was made using the Z transform technique and the results were compared to those of the LT model and the reference model described in section 4. The Z-transform model is indicated by ZT, the Laplace transform model by LT, and the reference model (semi-Lagrangian, semi-implicit) by SS.

The initial data were the same as were used in section 4. The difference between the ZT forecast at 24 h and the reference SS forecast, both using $\Delta t = 600$ s, is shown in Fig. 11a. This is very similar to the corresponding difference between the LT and SS forecasts (see Fig. 5). The rms differences in height and wind were 4.77 m and 0.82 m s^{-1} (compare 4.09 m and 0.64 m s^{-1} for LT versus SS). The difference between the 24-h forecasts of geopotential height made with the two transform integration schemes ZT and LT is shown in Fig. 11b. The rms differences in height and wind are now 1.27 m and 0.28 m s^{-1}, indicating that the two forecasts are virtually identical.

The two filtering schemes ZT and LT behave very similarly for small Δt. Forecasts for a larger time step $\Delta t = 1$ h were also made. Recall that the rms differences between the two forecasts using the LT model were 6.82 m for height and 1.37 m s^{-1} for wind. These were considered to be uncomfortably large, and it was pointed out in section 4 that the time truncation error was linear in Δt for the LT model. The corresponding
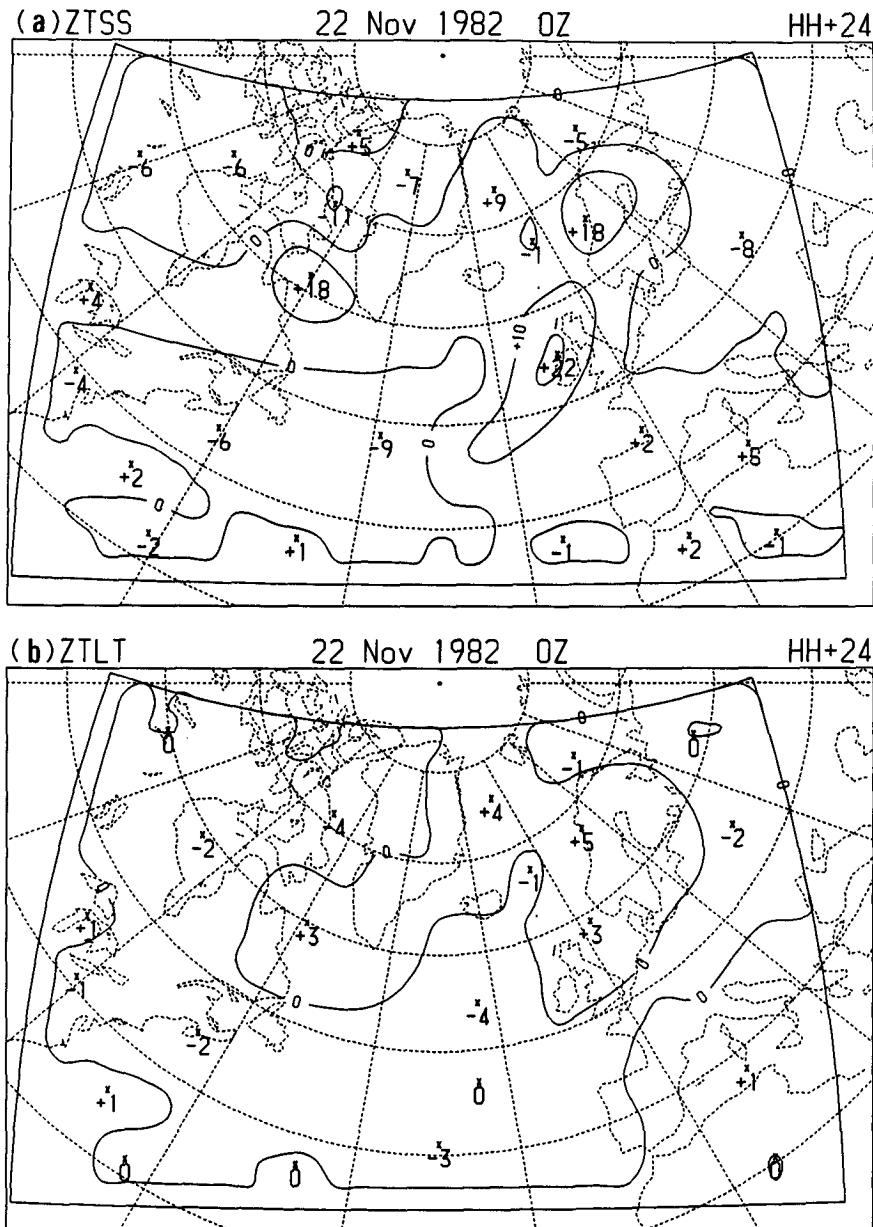
FIG. 11. (a) Difference between the 24-h height forecasts with the ZT model and the reference model SS. (b) Difference between the forecasts for the ZT and LT model.

time truncation errors for ZT were 9.59 m for height and 1.97 m s^{-1} for wind. Thus, although the integrations with the ZT scheme remain stable for large Δt, the errors are again larger than desirable for an operational scheme.

In conclusion, the behavior of the Z-transform scheme for small Δt is very like that of the LT scheme, and both models produce accurate and noise-free forecasts. However, the assumption that the advection terms are constant is made in deriving the transformed equations. This is acceptable for small time steps, but leads to a time truncation error which is linear in Δt. For both models the treatment of the advection terms

needs to be improved if accuracy for large time steps is to be achieved.

7. Discussion

A filtering integration scheme has been formulated using a modified form of the inversion integral for the Laplace transform (LT). This scheme eliminates the high-frequency components of the solution and provides a smooth evolution of the flow. Forecasts made with the LT scheme have been compared to those using a conventional scheme. With a small time step the two models produce very similar results, demonstrating that

the LT model is correctly simulating the flow while filtering out unimportant high frequency noise.

The Lagrangian treatment of advection permits the use of longer time steps without the onset of numerical instability. Although the integration of the LT model remained stable for large time steps, the accuracy of the forecast diminished significantly, with the time truncation error increasing linearly with Δt. An alternative filtering integration scheme, based on the Z transform, was formulated in the hope of reducing the time truncation errors. For small Δt the two filtering schemes behaved very similarly. Moreover, the ZT model also had errors which increased linearly with the time step. Thus far no success has been made in developing a filtering scheme with Lagrangian advection which has a quadratic error dependency on the time step.

A number of simple perturbation experiments showed that the LT model could assimilate data without the occurrence of high-frequency oscillations. A conventional semi-implicit model responded much more noisily to an imposed perturbation. The LT model is clearly superior in this regard, and is potentially useful for the problem of continuous data assimilation.

The LT model requires the solution of four (complex) Helmholtz equations per time step, and takes about six times longer to integrate than the reference model. The computational overhead might be much less for a scheme operating directly with the physical variables and not requiring transformations to the image space. It appears possible that such a scheme could be developed using the ideas of digital filtering (Hamming 1989).

Acknowledgments. Thanks to my colleague Dr. Aidan McDonald for numerous illuminating discussions. Thanks also to William K. Raymond and another reviewer for enlightened and helpful comments.

APPENDIX

Filtering with Z Transforms

The definition and elementary properties of the Z transform are presented and the method of filtering is described here. Further properties may be found in Doetsch (1971) or in books on digital signal processing, such as O'Flynn and Moriarty (1987) or Strum and Kirk (1988).

Consider a sequence $\{f_n\} = \{f_1, f_2, f_3, \cdots\}$. The Z transform of the sequence is defined as

$$\check{f}(z) \equiv \mathfrak{Z}\{f_n\} = \sum_{n=0}^{\infty} f_n z^{-n} \qquad (A.1)$$

and is a function of the complex variable z. For example, the transform of the constant sequence $\{1, 1, 1, \ldots\}$ is $z/(z-1)$; the exponential sequence $\{f_n = \alpha^n\}$ transforms to $z/(z-\alpha)$.

Equation (A.1) is a Laurent series for $\check{f}(z)$. The nth term is obtained by multiplying by z^{n-1} and integrating around a circle C_z centered at the origin and enclosing all the singularities of $\check{f}$. All terms but one vanish, giving

$$f_n = \mathfrak{Z}^{-1}\{\check{f}\} \equiv \frac{1}{2\pi i} \oint_{C_z} z^{n-1}\check{f}(z)dz. \qquad (A.2)$$

This is an expression for the inverse Z transform, allowing us to derive $\{f_n\}$ from $\check{f}(z)$.

From (A.1) it follows immediately that, if the transform of $\{f_n\}$ is $\check{f}$, the transform of the shifted sequence $\{f_{n+1}\}$ is $z(\check{f} - f_0)$. Thus, the transform of the finite difference $\Delta f_n = (f_{n+1} - f_n)$ is

$$\mathfrak{Z}\{\Delta f_n\} = (z-1)\check{f}(z) - zf_0. \qquad (A.3)$$

In this way a finite difference system transforms to an algebraic one, just as a differential equation becomes an algebraic one under the Laplace transform.

The discrete analogue of the oscillatory function $\exp(i\omega t)$ is α^n, where $\alpha = \exp(i\omega\Delta t)$ is unimodular. Low frequencies, that is small ω, correspond to α close to $z = 1$. Now consider a sequence with a number of oscillatory components

$$f_n = \sum_{k=1}^{K} c_k \alpha_k^n.$$

The Z transform of this function is

$$\check{f}(z) = \sum_{k=1}^{K} c_k \left(\frac{z}{z - \alpha_k}\right) \qquad (A.4)$$

which has poles at $z = \alpha_k$, with the lower frequency components corresponding to poles near $z = 1$ and higher frequencies mapping to points farther away on the unit circle. [The frequencies that can occur in a discrete system must fall in the Nyquist range $(-\omega_N, +\omega_N) = (-\pi/\Delta t, +\pi/\Delta t)$; the extreme values correspond to poles at $\exp(\pm i\pi)$.]

To retrieve $\{f_n\}$ from $\check{f}$, (A.2) may be applied. The integral has K contributions, from the poles at $z = \alpha_k$. To eliminate higher frequencies the circular contour C_z is replaced by a contour C_z^*, which encloses the poles close to $z = 1$ and excludes those further away:

$$f_n^* = \mathfrak{Z}^*\{\check{f}\} \equiv \frac{1}{2\pi i} \oint_{C_z^*} z^{n-1}\check{f}(z)dz. \qquad (A.5)$$

The contour C_z^* is chosen as the image of C_s^*, a circle of radius γ in the s plane under the mapping $z = \exp(s\Delta t)$ (see Fig. A1). The operator $\mathfrak{Z}^*\mathfrak{Z}$ thus acts as an ideal low-pass filter.

The character of the curve C_z^* depends on the nondimensional parameter

$$\Lambda = \tau_N/\tau_c = \gamma/\omega_N$$

where $\tau_N = 2\Delta t = 2\pi/\omega_N$ is the Nyquist period, the shortest period representable with time step Δt, and $\tau_c = 2\pi/\gamma$ is the cutoff period. For small Λ the curve
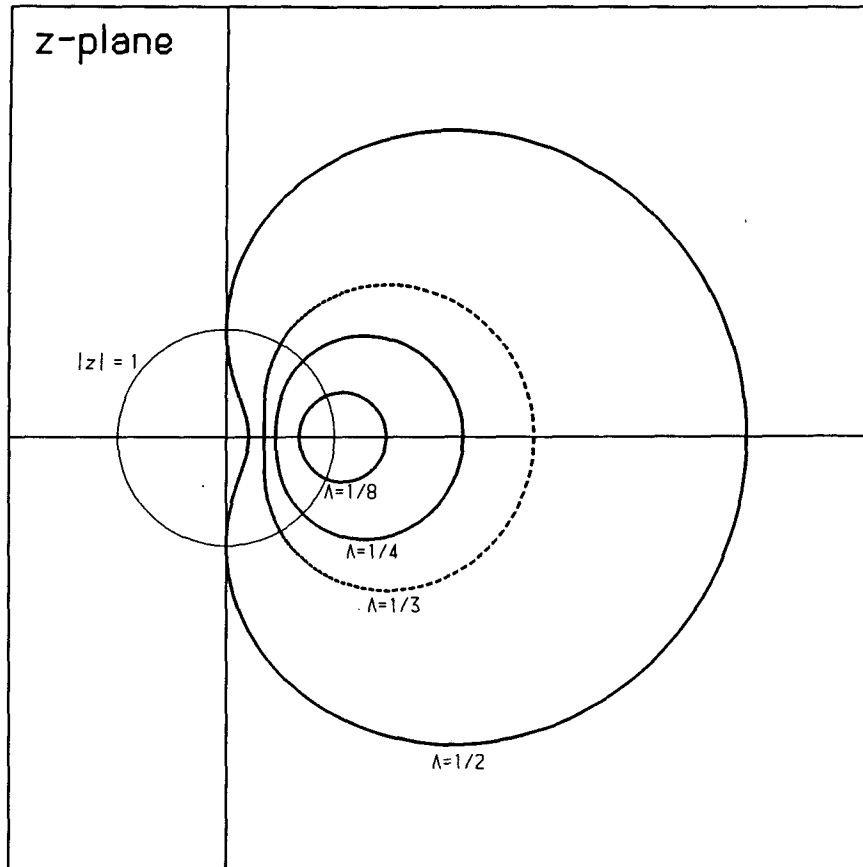
FIG. A1. Curves C_z^* used to calculate the modified inverse Z transform, $\mathfrak{Z}^*$, for various values of the nondimensional parameter Λ.

C_z^* is approximately circular. For large values of Λ it is distorted into a kidney shape (Fig. A1). For the experiments in section 5 $\tau_c = 6$ h was chosen; with a time step of 600 s, $\Lambda = \frac{1}{18}$ which is quite small; for a 1-h time step, $\Lambda = \frac{1}{3}$, corresponding to the dashed curve in Fig. A1.

There is a direct analogue between the modified inversion operator $\mathfrak{Z}^*$ and the modified inverse Laplace transform operator $\mathfrak{L}^*$. It is straightforward to show that, under the mapping $z = \exp(s\Delta t)$,

$$f_n^* = \mathfrak{Z}^*\{\tilde{f}(z)\} = \Delta t \mathfrak{L}^*\{\tilde{f}(e^{s\Delta t})\}|_{t=n\Delta t} \quad (A.6)$$

where $\mathfrak{L}^*$ is defined in section 2. To evaluate $\mathfrak{Z}^*$ numerically, $\tilde{f}[\exp(s_j\Delta t)]$ is calculated, where s_j is defined as before as the midpoints of the sides of an octogon (Fig. 2) and $\mathfrak{L}^*$ in (A.6) is replaced by a summation over j.

REFERENCES

Daley, R., 1980: The development of efficient time integration schemes using normal mode models. *Mon. Wea. Rev.*, **108**, 100–110.

——, 1981: Normal mode initialization. *Rev. Geophys. Space Phys.*, **19**, 450–468.

Doetsch, G. 1971: *Guide to the Applications of the Laplace and Z Transforms*. Van Nostrand Reinhold, 240 pp.

Hamming, R. W., 1989: *Digital Filters*, 3rd Ed., Prentice-Hall, 284 pp.

Lynch, Peter, 1985a: Initialization using Laplace transforms. *Quart. J. Roy. Meteor. Soc.*, **111**, 243–258.

——, 1985b: Initialization of a barotropic limited area model using the Laplace transform technique. *Mon. Wea. Rev.*, **113**, 1338–1344.

——, 1986: Numerical forecasting using Laplace transforms: Theory and application to data assimilation. Technical Note No. 48. 32 pp. [Available from Irish Meteorological Service, Glasnevin Hill, Dublin 9, Ireland.].

O'Flynn, M., and E. Moriarty, 1987: *Linear Systems: Time Domain and Transform Analysis*. John Wiley and Sons, 500 pp.

McDonald, A., 1986: A semi-Lagrangian and semi-implicit two time-level integration scheme. *Mon. Wea. Rev.*, **114**, 824–830.

——, and J. R. Bates, 1987: Improving the estimate of the departure point in a two time-level semi-Lagrangian and semi-implicit scheme. *Mon. Wea. Rev.*, **115**, 737–739.

Swartztrauber, P., and R. Sweet, 1975: Efficient FORTRAN subprograms for the solution of elliptic partial differential equations. NCAR, Tech. Note IA-109, 139 pp.

Strum, R. D., and D. E. Kirk, 1988: *Discrete Systems and Digital Signal Processing*. Addison-Wesley, 848 pp.

Van Isacker, J., and W. Struylaert, 1985: Numerical forecasting using Laplace transforms. *Publications Serie A*, **115**. 32 pp. [Available from Royal Belgian Meteorological Institute, Ave. Circulaire 3, Brussels, Belgium.].

——, and ——, 1986: Laplace transforms applied to a baroclinic model. *Short- and Medium-Range Numerical Weather Prediction*. Proc. of IUGG NWP Symposium, 247–253 Meteorological Society of Japan, T. Malsuno, Ed., 831 pp.